the *Chandra* podcasts were converted to the Adobe Media Player (AMP) format for the launch of the AMP channel on NASA's website. The team received a NASA ROSES grant to implement the International Year of Astronomy Cornerstone Project, "From Earth to the Universe" exhibits at two semi-permanent and six traveling sites around the United States (see the "*Chandra* in IYA2009" article).

We look forward to a new year of continued smooth operations and exciting science results. Please join us to celebrate *Chandra*'s discoveries at the seminar Ten Years of Science with *Chandra*, to be held in Boston in September, 2009. ✯

Instruments: ACIS

Paul Plucinsky, Catherine Grant, Joe DePasquale

The ACIS instrument continued to perform well over the past year with no failures or unexpected degradations. The charge-transfer inefficiency (CTI) of the FI and BI CCDs is increasing at the expected rate. The CIAO software and associated calibration files correct for this slow increase in CTI over time. The contamination layer continues to accumulate on the ACIS optical-blocking filter. Recent measurements indicate that a revision of the temporal model for the contaminant may be necessary. The CXC calibration group is investigating the issue and may release a revision later this year.

The only significant change in ACIS performance over the last year regards the thermal control of the ACIS focal plane (FP). As discussed in last year's newsletter article, a higher percentage of ACIS observations have been experiencing warmer than desired FP temperatures as the spacecraft ages and components inside the spacecraft get warmer in general. In response to this trend the ACIS Operations team turned off the ACIS Detector Housing (DH) heater on April 7, 2008. Before the DH heater was turned off, approximately 1/3 of observations had an average FP temperature of -119.2 C or warmer. After the DH heater was turned off, only about 2% of observations had an average FP temperature of -119.2 C or warmer. The desired FP temperature is -119.7 C. The FI CCDs have a narrower tolerance on the FP temperature than the BI CCDs. For the FI CCDs, the gain changes by 0.3% at 1.5 keV if the FP temperature warms to -119.2 C and for the BI CCDs, the gain changes by 0.3% if the FP temperature increases to -118.2 C. Figure 6 shows the average FP temperature from April 2007 until January 2009. The red line shows the FI CCD limit of -119.2 C and the blue line shows the BI CCD limit of -118.2 C. The figure clearly demonstrates the improvement in control of the ACIS FP temperature since the DH heater was turned off.

As a consequence of this change, the temperature of the ACIS Camera Body (CB) is no longer actively controlled. This created a complication for the aspect reconstruction since the ACIS fiducial lights are mounted on the ACIS CB. As the CB temperature increases/decreases the CB expands/contracts, producing an apparent motion in the fiducial lights. The CXC Aspect team has calibrated this motion by relating the brightness of the fiducial lights to the CB temperature and has modified the aspect reconstruction software to account for this effect. After applying this change, the Aspect team has confirmed that the aspect reconstruction is as accurate after the DH heater was turned off as it was before. ✯

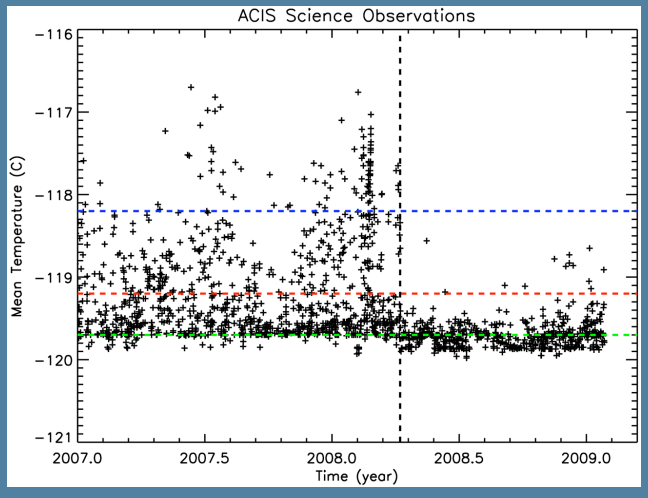

FIGURE 6: The average ACIS focal plane temperature for science observations from April 2007 until January 2009. The dashed vertical line at 2008.27 indicates the day on which the ACIS detector housing heater was turned off. The green dashed horizontal line indicates the desired FP temperature of -119.7 C. The red dashed line indicates the temperature (-119.2 C) at which the gain of the FI CCDs changes by 0.3% and the blue dashed line indicates the temperature (-118.2 C) at which the gain of the BI CCDs changes by 0.3% .

Instruments: HRC

Ralph Kraft, C.-Y. Ng

HRC operations continue smoothly with no major problems, anomalies, or interruptions. Routine monitoring observations show no significant charge extraction from the detectors. There may be some evidence of a decrease in the low energy (below 400 eV) QE of the HRC-S, probably indicative of the chemical evolution of

the CsI photocathode. This is being monitored by the CXC Cal team and the HRC instrument team, but this phenomenon currently is not significant for scientific observations. There has been no significant change in the HRC-I quantum efficiency during the past year. One HRC observation was made using one of the shutters during the past year, an HRC+LETG observation of the Crab Nebula. The shutter was used to block the zeroth order image in order to reduce the overall instrument rate from this bright source below the telemetry limit. There were some anomalies in inserting and withdrawing the shutter in the past. Overall another quiet year from an HRC perspective.

A wide variety of scientific investigations have been carried out over the past year with the HRC instruments. This year we highlight an HRC-I observation of the Mouse nebula, a pulsar wind nebula, demonstrating the HRC's imaging and timing capabilities.

High Resolution X-ray Imaging of the Mouse

C.-Y. Ng, for the Mouse Team

Neutron stars lose a significant amount of their rotational energy through the relativistic winds. The consequent interactions with the surrounding materials result in broadband synchrotron emission, collectively referred to as pulsar wind nebulae (PWNe). The properties of PWNe depend strongly on the evolutionary state and environment. Since neutron stars are typically born with space velocities of a few hundred kilometers per second, they eventually escape the natal supernova remnants and travel supersonically through the interstellar medium. This results in bow shock nebulae, in which a pulsar's relativistic outflow is confined by the ram pressure. As compared to PWNe confined within supernova remnants, bow shocks are governed by a much simpler set of boundary conditions, offering ideal cases to refine our understanding of relativistic shocks and pulsar winds electrodynamics.

The best example of a bow shock PWN is G359.23-0.82 ('the Mouse') powered by the 0.1s period pulsar J1747-2958. This is the brightest bow shock system in X-rays, located near the direction of the Galactic center. Multi-wavelength studies show that the Mouse is well-modeled by a bright 'head' coincident with the pulsar, a 'tongue' corresponding to the surface of the wind termination shock, and an elongated 'tail' produced by material in the post-shock flow. We have recently obtained new HRC observations of this bow shock system, which offers the highest angular resolution images. Figure 7 shows the HRC image (raw and smoothed, respectively), demonstrating the unique capability of the HRC instrument. The new HRC observation suggests some hints of small-scale features, possibly a jet or knots, near the backward termination shock. The results will allow a comparison to detailed magnetohydrodynamic simulations. For comparison, an archival ACIS images of the same region is shown in Figure 8. For timing analysis, we have carried out simultaneous radio timing observations of the central pulsar in order to fold the HRC data. The lightcurve of the pulsar is shown in Figure 9 folded on the frequency of the radio pulsations (100 ms). We found no statistically significant X-ray pulsation at the radio pulse frequency. ✭

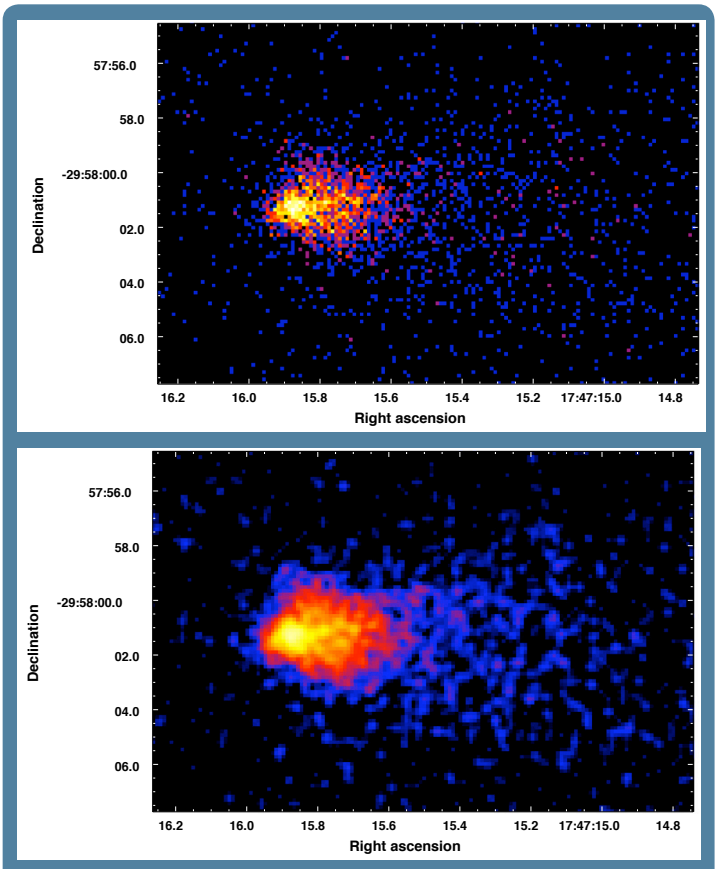

FIGURE 7: Raw (top) and smoothed (bottom) HRC-I images of the Mouse PWN.

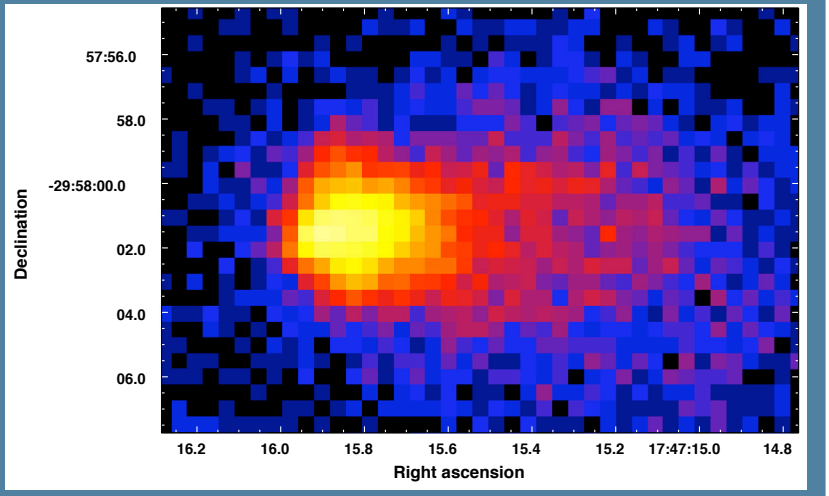

FIGURE 8: ACIS-S image of the Mouse PWN.

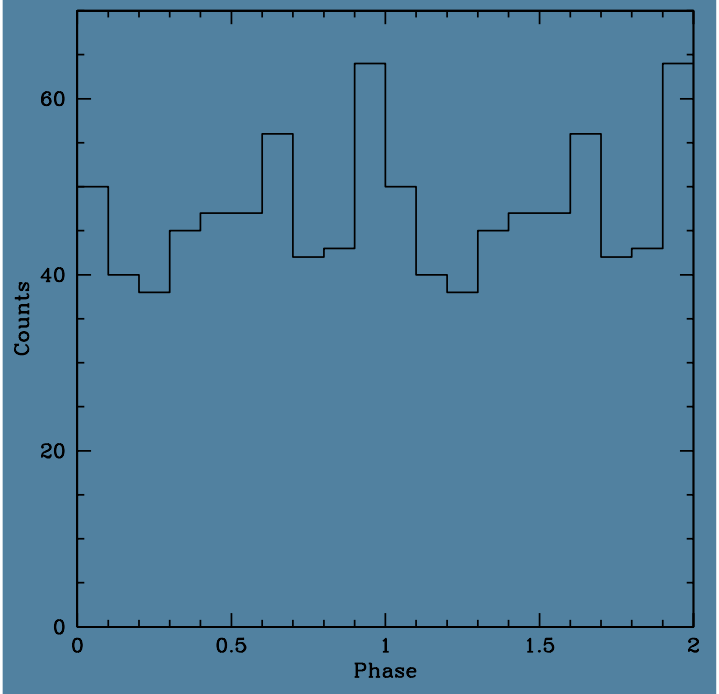

FIGURE 9: HRC-I lightcurve of the central pulsar of the Mouse PWN folded on the frequency of the radio pulsations.

Be sure to also see the TGCat article in this Newsletter !

INSTRUMENTS: HETG

DAN DEWEY

HETG Status and Calibration

The HETG continues to perform nominally with no specific issues. Of note in the past year are the efforts of the "International Astronomical Consortium for High Energy Calibration" (http://www.iachec.org/) to assess the cross-calibration of several current X-ray missions. HETG observations contributed to the low-energy results given in: "The SMC SNR 1E0102.2-7219 as a Calibration Standard for X-ray Astronomy in the 0.3-2.5 keV Bandpass" by Plucinsky et al. 2008. The missions (and instruments) included in this paper are: *XMM-Newton* (RGS1, MOS1, MOS2, pn), *Chandra* (HETG-MEG, ACIS-S3), *Suzaku* (XIS0, XIS1) and *Swift* (XRT). Relative flux measurements were compared at four low-energy spectral regions, corresponding to the bright lines of O VII, O VIII, Ne IX and Ne X (with rough energies of 0.57, 0.65, 0.92, and 1.02 keV.) These mid-2008 results demonstrate an absolute calibration agreement that is largely within ±10% across the instruments. The effort is on-going with yearly IACHEC meetings, the next is scheduled for the end of April 2009.

HETG Technique: "Look Ma! No Angstroms!"

HETG spectra are often presented in counts versus Angstrom space and plotted to emphasize narrow spectral features, and so they look very different when compared with X-ray spectra from CCD instruments (e.g., ACIS, EPIC, XIS). However, there is nothing about the HETG spectral products that prevents viewing them in the more familiar flux versus keV space. Likewise, as the following examples show, HETG observations can be used to: measure continuum sources, create light curves, generate hardness ratios, etc.

The broadband MEG spectrum of the Galactic X-ray binary 4U 1957+11 is shown in Figure 10; this binary includes what may be the most rapidly spinning black hole in the Galaxy. Here the data are fit with a model consisting of a disk blackbody plus a Comptonizing corona which contributes at higher energies. Besides studying black hole emission models through the broadband spectra, the data also allowed for a very accurate (and very low) determination of the N_H toward 4U 1957. Of course one can still zoom in on the spectrum and study narrow features that may be present. For example, here Ne IX absorption is seen at about 0.92 keV. The measured depth of this feature is consistent with the idea that most of the hot gas we see

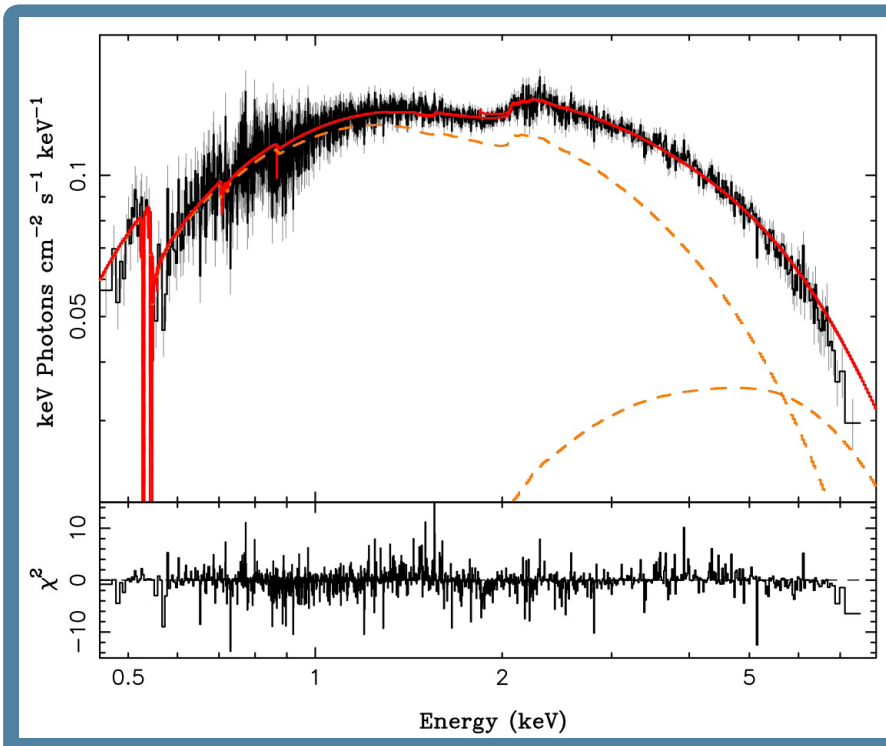

FIGURE 10: HETG spectrum of the low-mass X-ray binary 4U 1957+11. See text for discussion. (from Nowak et al. 2008)